ELSEVIER

Nuclear Instruments and Methods in Physics Research A 450 (2000) 495–514

NUCLEAR INSTRUMENTS & METHODS IN PHYSICS RESEARCH Section A

www.elsevier.nl/locate/nima

Gamma-ray spectroscopy on irradiated MTR fuel elements

L.A.A. Terremoto*, C.A. Zeituni, J.A. Perrotta, J.E.R. da Silva

Instituto de Pesquisas Energéticas e Nucleares (IPEN/CNEN-SP); Divisão de Engenharia do Núcleo (REN); Travessa R, 400 – Cidade Universitária; Caixa Postal 11.049; CEP 05422-970; São Paulo – SP, Brazil

Received 16 March 1999; received in revised form 5 November 1999; accepted 21 December 1999

Abstract

The availability of burnup data is an important requirement in any systematic approach to the enhancement of safety, economics and performance of a nuclear research reactor. This work presents the theory and experimental techniques applied to determine, by means of nondestructive gamma-ray spectroscopy, the burnup of Material Testing Reactor (MTR) fuel elements irradiated in the IEA-R1 research reactor. Burnup measurements, based on analysis of spectra that result from collimation and detection of gamma-rays emitted in the decay of radioactive fission products, were performed at the reactor pool area. The measuring system consists of a high-purity germanium (HPGe) detector together with suitable fast electronics and an on-line microcomputer data acquisition module. In order to achieve absolute burnup values, the detection set (collimator tube + HPGe detector) was previously calibrated in efficiency. The obtained burnup values are compared with ones provided by reactor physics calculations, for three kinds of MTR fuel elements with different cooling times, initial enrichment grades and total number of fuel plates. Both values show good agreement within the experimental error limits.

PACS: 29.30.Kv; 28.41.Bm; 28.41. − i; 28.50.Dr

Keywords: Gamma spectroscopy; Fuel elements; Research reactors; Fission products

1. Introduction

Gamma-ray spectroscopy is a nondestructive method for measuring the relative distributions of fission products in irradiated fuel elements. To obtain the necessary information, complete gamma-ray spectra are accumulated as a function of axial and transversal positions. The net areas under the full-energy peaks are determined, giving a quantitative measurement of the amount of each radioactive fission product present at a specific location. These amounts can be related to the total absolute activity of a given fission product, used as burnup monitor, which enables the determination of the total number of fission events and therefore the fuel element absolute burnup. Such determination, however, requires the previous energy and efficiency calibration of the experimental apparatus, a rigorous control of its geometry, detailed knowledge about the irradiation history of the fuel element and accurate evaluation of all attenuation effects involved. Table 1 shows the most suitable nuclides for use as burnup monitors [1–5].

* Corresponding author. Tel.: + 55118169439; fax: + 55118169432.

E-mail address: laaterre@net.ipen.br (L.A.A. Terremoto).

0168-9002/00/$ - see front matter
PII: S0168-9002(00)00250-3

Table 1
Main properties of the fission products used as burnup monitors in gamma-ray spectroscopy measurements on irradiated fuel elements: fuel element history (concerning irradiation and cooling periods), fission product used as standard burnup monitor, half-life $T_{1/2}$, energy E_γ and absolute emission intensity I_γ of the main emitted gamma-rays, fission yield for ^{235}U, ^{238}U and ^{239}Pu by thermal neutrons y_t and by fast neutrons y_r [3–5]. In the case of ^{235}U, y is the average fission yield of the burnup monitor, resulting from average of y_t and y_r weighted on the mean values of the thermal and fast neutron fluxes in the IEA-R1 research reactor

Fuel element history		Burnup monitor	$T_{1/2}$	E_γ (keV)	I_γ	^{235}U			^{238}U	^{239}Pu	
Irradiation	Cooling					y_t (%)	y_r (%)	y (%)	y_r (%)	y_t (%)	y_r (%)
< 40 d	> 9 d	^{140}Ba/^{140}La	12.75 d	1596.5	1.099	6.30	6.13	6.18 ± 0.13	5.98	5.56	5.29
< 200 d	> 40 d	^{95}Zr	64.03 d	724.2	0.437	6.49	6.37	6.41 ± 0.09	5.13	4.89	4.66
				756.7	0.554						
≥ 1000 d	< 2 yr	^{144}Ce/^{144}Pr	284.9 d	2185.7	0.007	5.48	5.28	5.34 ± 0.16	4.50	3.74	3.74
> 1800 d	≥ 2 yr	^{137}Cs	30.14 yr	661.6	0.851	6.21	6.16	6.18 ± 0.04	5.97	6.62	6.49

Once the fission yield of the burnup monitors vary considerably with the fissionable nuclide, it is necessary to evaluate the total amount of fission events due to ^{235}U, ^{238}U and ^{239}Pu in a given irradiated nuclear fuel.

Concerning the initial enrichment grade, nuclear fuels already irradiated in IEA-R1 core are of two types [6]: (a) 93.15% enrichment fuels, designated as High Enriched Uranium (HEU) fuels; (b) 19.75% enrichment fuels, designated as Low Enriched Uranium (LEU) fuels. Fission events in irradiated HEU fuels are essentially due to ^{235}U. Calculations performed with the code ORIGEN 2 [7] show that this assumption is valid also for LEU fuels irradiated under the typical conditions [8] found inside the IEA-R1 core at 2 MW. In this case, if fission events due to ^{238}U and ^{239}Pu are neglected, the associated uncertainty is lower than the minimal total relative error of $\pm 3.1\%$ estimated [2] for burnup determination by means of gamma-ray spectroscopy.

The standard fuel elements used in the IEA-R1 research reactor are plate type, usually designated as Material Testing Reactor (MTR) fuel elements. A typical fuel element has 18 plane parallel fuel plates, mounted mechanically between two lateral aluminum holders with grooves, and its overall dimensions are (7.6×8.0) cm by 88.0 cm high. Each fuel plate consists of an aluminum cladding and a meat, where the fuel material is located, containing approximately 10 g of ^{235}U. The fuel plate total thickness is 0.152 cm, and the distance between two successive plates is 0.289 cm. Fig. 1 shows the cross-sectional diagram of a standard MTR fuel element and the structure of two successive fuel plates in it.

2. Theory

2.1. Corrections due to attenuation effects

The irradiation of fuel elements gives rise to radioactive fission products that, in the absence of cladding failures, remain inside the meat of each fuel plate. These fission products emit gamma-rays, which are attenuated as they emerge from the irradiated fuel and traverse successive layers of different materials.

Evaluation of effects caused by attenuation of gamma-rays is necessary to determinate the absolute gamma activity of irradiated fuel elements. Corrections due to attenuation effects are calculated using the reference frame shown in Fig. 1 regarding an horizontally positioned fuel element.

The first correction to be calculated results from the attenuation of gamma-rays traversing the plate meat where they are emitted. This effect is called self-attenuation, and the correction associated needs two hypothesis to be calculated, both based on characteristics of the experimental apparatus: (a) once the detector is positioned far away from the point where the gamma-ray was emitted, the radiation is strongly directed along the Z-axis; (b) once

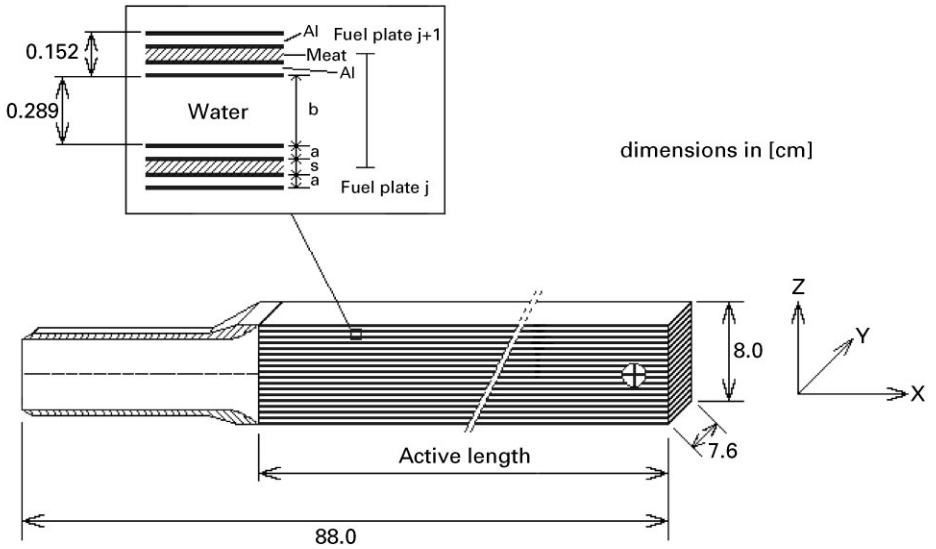

Fig. 1. Cross-sectional diagram of a standard MTR fuel element irradiated in the IEA-R1 research reactor, showing in detail the structure of two successive fuel plates. The position of the reference frame used is indicated. Dimensions of a (aluminum cladding thickness), s (plate meat thickness) and active length are shown in Table 7.

the geometry of the detection set (collimator tube + gamma-ray detector) remains unchanged, the detection solid angle Ω is the same for every point of the emitting source. The self-attenuation correction is given by [9]

$$k_1 = \frac{1 - e^{-\mu s}}{\mu s} \tag{1}$$

where s is the plate meat thickness and μ is the linear attenuation coefficient, for a given gamma-ray energy, of the fuel material contained in the plate meat.

A second correction is due to attenuation that arises when gamma-rays pass through the fuel plates and the water between them, because measurements have to be performed at the reactor pool. In order to calculate this correction, two hypothesis are made: (a) once all fuel plates of an element are identical and were irradiated under the same conditions, the specific activity ρ related to each one of the 18 fuel plates, along the Z-axis, is the same for a point (x, y); (b) once the detector is positioned far away from the point where the gamma-ray was emitted and taking into account the presence of a collimator tube, the radiation is strongly directed along the Z-axis.

Fig. 1 shows schematically the different layers that exist between two successive fuel plates of an immersed fuel element.

Considering this configuration, the correction that corresponds to the attenuation of a gamma-ray, emitted in the meat of the jth fuel plate and passing through successive layers until reaching the upper surface of the meat contained inside the last (18th) fuel plate, results

$$F_j = (e^{-2\mu_{Al}a} e^{-\mu_a b} e^{-\mu s})^{18-j} = K^{18-j} \tag{2}$$

where μ_{Al} is the aluminum linear attenuation coefficient, μ_a is the water linear attenuation coefficient, a is the aluminum cladding thickness, s is the plate meat thickness and b is the water layer thickness.

The next correction to be evaluated arises from the attenuation of a gamma-ray after traversing the upper aluminum cladding of the last fuel plate, the water layer between the last fuel plate and the bottom edge of the collimator tube and afterwards the aluminum window that closes the collimator tube (see Fig. 2). In this case, the correction due to

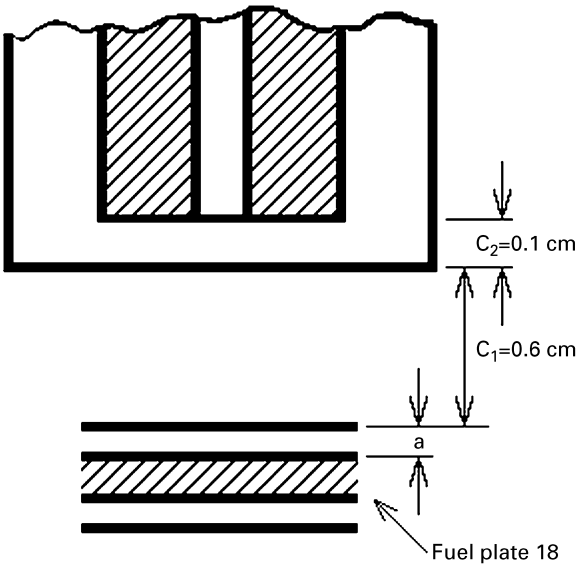

Fig. 2. Structure of the different layers that exist between the last fuel plate of an immersed fuel element and the bottom end of the collimator tube. Dimensions of a (aluminum cladding thickness) are shown in Table 7.

attenuation is given by

$$k_2 = e^{-\mu_{Al} a} e^{-\mu_a C_1} e^{-\mu_{Al} C_2} \quad (3)$$

where C_1 is the distance between the last fuel plate and the bottom edge of the collimator tube and C_2 is the thickness of the aluminum window.

Finally, the gamma-ray passes through the air contained inside the collimator tube before it strikes the detector. As a consequence of the attenuation, another correction must be considered:

$$k_3 = e^{-\mu_{air} L} \quad (4)$$

where μ_{air} is the linear attenuation coefficient of air and L is the total length of the collimator tube.

The total correction due to attenuation of a gamma-ray that, once emitted in the meat of the jth fuel plate, is allowed to strike a detector after passing through the different layers mentioned, can be obtained from the product of all corrections already calculated. As a consequence, if $\rho(x, y)$ is the specific activity of the irradiated fuel plates at the point (x, y), the number of counts per unit of time registered by the detector due to the jth fuel plate, when the collimator tube is positioned over the point (x, y), is equal to

$$Q_j(x, y) = \rho(x, y) a_j s I_\gamma \varepsilon_\gamma k_1 k_2 k_3 K^{18-j} \quad (5)$$

where a_j is the area defined by the detection solid angle on the central plane of the jth plate meat, s is the meat thickness, I_γ is the absolute emission intensity of the gamma-ray and ε_γ is the intrinsic efficiency of the HPGe detector for gamma-rays of a given energy.

Considering the activity of all the 18 fuel plates of an irradiated fuel element, the total number of counts per unit of time registered by the detector, results

$$Q(x, y) = \sum_{j=1}^{18} Q_j(x, y) = \rho(x, y) s I_\gamma \varepsilon_\gamma k_1 k_2 k_3 \sum_{j=1}^{18} a_j K^{18-j} \quad (6)$$

If l is the active length of each fuel plate of the element, w is the active width of each fuel plate of the element and $\bar{\rho}$ is the average specific activity of each fuel plate, the total activity of a fuel element due to a burnup monitor is

$$D = 18 l w s \bar{\rho}. \quad (7)$$

On the other hand, the average value $\overline{Q}$ for the total number of counts per unit of time registered in the detector is obtained by means of measurements performed along the active length and along the active width of the fuel element, been related to $\bar{\rho}$ by the expression

$$\overline{Q} = \bar{\rho} s I_\gamma \varepsilon_\gamma k_1 k_2 k_3 \sum_{j=1}^{18} a_j K^{18-j}. \quad (8)$$

Using expressions (7) and (8), the total activity of a fuel element due to a burnup monitor can be written as

$$D = \frac{18 l w \overline{Q}}{I_\gamma \varepsilon_\gamma k_1 k_2 k_3 \sum_{j=1}^{18} a_j K^{18-j}}. \quad (9)$$

Expression (9) shows that, once the total correction due to attenuation effects has been considered, it is necessary to measure the values of ε_γ, a_j and $\overline{Q}$ in order to determinate experimentally the total activity D of the irradiated fuel element that corresponds to a given burnup monitor.

2.2. Burnup determination

The values of ε_γ and a_j are measured during the efficiency calibration of the experimental apparatus. Regarding the parameter $\overline{Q}$, its value must be measured to determinate experimentally the total activity of the irradiated fuel element due to a given burnup monitor and, thereafter, the fissioned mass of ^{235}U in this fuel element. The ratio between fissioned and initial masses of ^{235}U in a fuel element furnishes its burnup.

As mentioned before, the average value $\overline{Q}$ for the total number of counts per unit of time registered in the detector is obtained by means of measurements performed along the active length (X-axis) and along the active width (Y-axis) of the fuel element. These measurements define a function of two variables, with typical profiles like the ones shown in Fig. 3.

Applying a property of two-variable functions [10] to the experimentally obtained profiles, one finds

$$\overline{Q} = \overline{P_x} + \overline{P_y} - Q \tag{10}$$

where $\overline{P_x}$ is the average number of counts per unit of time obtained in measurements along the fuel element active length, $\overline{P_y}$ is the average number of counts per unit of time obtained in measurements along the fuel element active width and Q is the number of counts per unit of time measured at the central point of the fuel element. Replacing this formulation for $\overline{Q}$ in expression (9), and using the radioactive decay law, the total number of burnup monitor nuclei present in the fuel, immediately after the end of the last irradiation period, becomes

$$N_0 = \frac{18lw(\overline{P_x} + \overline{P_y} - Q)}{\lambda I_\gamma \varepsilon_\gamma k_1 k_2 k_3 \sum_{j=1}^{18} a_j K^{18-j}} e^{\lambda t_c} \tag{11}$$

where λ is the decay constant of the burnup monitor and t_c is the time interval between the end of the last irradiation period and the start of the measurements on it.

The fissioned mass of ^{235}U in the irradiated fuel element is given by

$$\Delta U = \frac{N_0 m_0}{y N_U^0} f \tag{12}$$

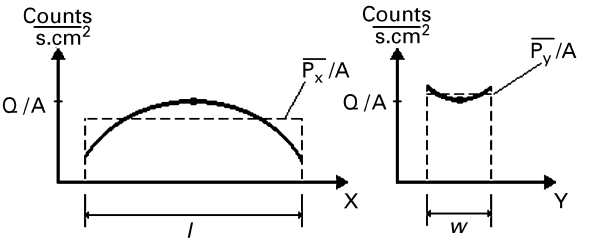

Fig. 3. Representation of typical burnup profiles obtained from gamma-ray spectroscopy measurements on irradiated MTR fuel elements. The parameters indicated are employed to calculate the average value $\overline{Q}$.

where N_U^0 is the initial number of ^{235}U atoms in the fuel element, m_0 is the initial mass of ^{235}U in the fuel element, y is the average yield of the burnup monitor in the fission of ^{235}U (see Table 1) and f is a correction factor that takes into account the decay of burnup monitor nuclei occurred during different irradiation periods and powers, which is given by the following expression [11]:

$$f = \frac{\lambda \sum_{k=1}^{n} P_k t_k}{\sum_{k=1}^{n} P_k e^{-\lambda \tau_k}(1 - e^{-\lambda t_k})}, \tag{13}$$

where λ is the decay constant of the burnup monitor, P_k is the average relative power corresponding to the kth irradiation period (been $\sum_{k=1}^{n} P_k = 1$), n is the total number of irradiation periods during the whole irradiation history of the fuel element, t_k is the duration of the kth irradiation period and τ_k is the time interval between the end of the kth irradiation period and the end of the last irradiation period.

Finally, the combined use of Eqs. (11)–(13) determines the fissioned mass of ^{235}U in the irradiated fuel element, while the ratio $\Delta U/m_0$ furnishes its burnup.

3. Experiment

3.1. Experimental apparatus

The experimental apparatus for gamma spectroscopy consists of collimator tube, lead shielding, high-purity germanium (HPGe) detector together

with fast suitable electronics and an on-line microcomputer data acquisition module. The collimator tube is positioned between the irradiated fuel element and the detector in order to enable the determination of the gamma emission rate of a specific fuel volume, as well as to avoid the system overflow concerning data acquisition.

Fig. 4 shows schematically the cross-sectional diagram of the collimator tube used in the gamma-ray spectroscopy measurements.

After been collimated, gamma-rays are detected by the electronic components presented in Table 2. These electronic components are specially designed for nuclear spectroscopy applications with ultra-high input counting rates (exceeding 200,000 counts/s). Moreover, the HPGe detector employed in the measurements has an ultra-high count-rate preamplifier (transistor-reset preamplifier) which can handle input counting rates up to 1,000,000 counts/s at 1 MeV.

In this work, the highest gross counting rate registered in a complete spectrum obtained from gamma-ray spectroscopy on irradiated fuel elements (see part 3, Section 3.5, as well as part 4) was 742.2 counts/s, which lays far bellow the above-mentioned rates.

The HPGe detector has a volume of 130 cm^3, with 1.71 keV resolution and 26.1% relative efficiency for the 1332.5 keV gamma-ray of ^{60}Co [12]. The gamma-ray energy range taken for the analysis was from 50 to 2800 keV.

3.2. Measurement of the intrinsic efficiency ε_γ

Before the burnup measurements, it is necessary to measure the intrinsic efficiency ε_γ of the HPGe detector at the gamma-ray energies of interest.

The intrinsic efficiency of a detector usually depends primarily on the detector material, the radiation energy, and the physical thickness of the detector in the direction of the incident radiation. Therefore, the intrinsic efficiency has a slight dependence on the average path length of the radiation through the detector [13].

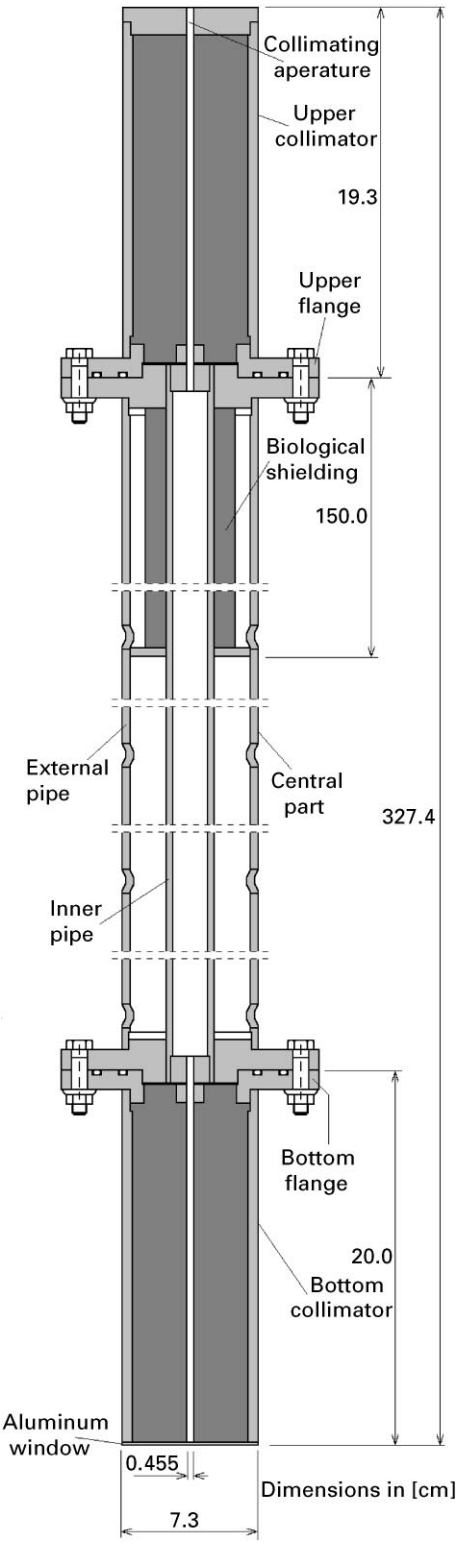

Fig. 4. Cross-sectional diagram of the collimator tube used in the gamma-ray spectroscopy measurements.

Table 2
Main electronic components of the experimental apparatus

Measuring system components		
Component	Model	Manufacturer
HPGe detector	GEM-25185-P-PLUS	
Amplifier	973U	
High voltage supply	659	EG&G ORTEC
BIN	4001C	
Multichannel analyzer	921 SPECTRUM MASTER	

Regarding the HPGe detector used in the experiment, this fact causes the intrinsic efficiency to vary when measured allowing gamma-rays of a given energy to strike the entire face of the detector crystal or a small area in its center. Such changes in efficiency, however, are quite small for high-energy gamma-rays impinging on the close-ended coaxial configuration of the detector. Hence, it was decided to measure the intrinsic efficiency of the HPGe detector without collimating the gamma-rays and following the procedure described along this section.

In order to measure the parameter ε_γ, the HPGe detector was fixed at the upper part of a cylindrical lead shielding with a side opening that enables the one-by-one centralized positioning of punctiform calibration sources inside. The main characteristics of these calibration sources are shown in Table 3. During the measurements, the distance between the center of the HPGe detector window and the center of each calibration source was constant and equal to $h = 6.575$ cm. The only exception was the measurement performed with the ^{226}Ra source, during which $h = 19.045$ cm. In this case, the distance h was enlarged to assure that sum-coincidence effects [13] do not affect the measurement. The attenuation enhancement due to the larger distance used is negligible, once only the higher energy gamma-rays emitted were considered.

A gamma spectrum was obtained for each calibration source in runs of 60 s live time. The full-energy peaks of each spectrum were fitted by Gaussian function plus a parabolic curve for the continuous background using the computer code IDEFIX [14]. By means of this procedure, the net number of counts (Area) under each full-energy peak was determined and therefore the intrinsic efficiency ε_γ of the HPGe detector at the gamma-ray energies emitted by the calibration sources.

The intrinsic efficiency ε_γ was calculated as

$$\varepsilon_\gamma = \frac{\text{Area}}{GATI_\gamma} \tag{14}$$

where A is the calibration source activity at the measurement start, T is the live time of measurement, I_γ is the gamma-ray absolute emission intensity and G is the geometric correction factor. In the configuration of the measurement, where the detector is cylindrical, the calibration source is punctiform, the distance detector/source remains unchanged and the centers of both are aligned, the geometric correction factor results [15]

$$G = \frac{1}{2}\left\{1 - \frac{(h+g)}{[(h+g)^2 + R^2]^{1/2}}\right\} \tag{15}$$

where R is the radius of the germanium crystal base contained inside the HPGe detector and g is the width of the gap between the aluminum window and the crystal base in the detector. The dimensions of the HPGe detector [9] are $R = 2.760$ cm and $g = 0.300$ cm.

The obtained values of the intrinsic efficiencies ε_γ at the gamma-ray energies E_γ emitted by the calibration sources are shown in Table 4. These data were fitted by a function with the following general expression [16]:

$$\ln \varepsilon_\gamma = a_0 + a_1 \ln\left(\frac{E_\gamma}{E_r}\right) + a_2\left[\ln\left(\frac{E_\gamma}{E_r}\right)\right]^2 + a_3\left[\ln\left(\frac{E_\gamma}{E_r}\right)\right]^3 \tag{16}$$

Table 3
Main characteristics of the punctiform calibration sources utilized in the determination of ε_γ [4,13]: half-life $T_{1/2}$, initial activity A_0, gamma-ray energy E_γ, gamma-ray absolute emission intensity I_γ, manufacture date

Source	$T_{1/2}$	A_0 (kBq)	E_γ (keV)	I_γ	Manufacture date (day/month/year)
^{22}Na	2.60 yr	379 ± 15	1274.6	0.9990	01/05/1996
^{54}Mn	312.5 d	447 ± 18	834.8	1.0000	01/05/1996
^{57}Co	271.8 d	452 ± 18	122.0	0.8560	01/05/1996
			136.5	0.1060	
^{60}Co	5.27 yr	473 ± 19	1173.2	0.9990	01/05/1996
			1332.5	1.0000	
^{88}Y	106.6 d	396 ± 16	898.0	0.9400	01/05/1996
			1836.1	0.9940	
^{133}Ba	10.54 yr	396 ± 20	160.6	0.0072	01/05/1996
			223.1	0.0047	
			276.4	0.0729	
			302.9	0.1860	
			356.0	0.6230	
			383.9	0.0884	
^{137}Cs	30.14 yr	421 ± 17	661.6	0.8510	01/05/1996
^{152}Eu	13.33 yr	66 ± 2	121.8	0.2840	01/04/1991
			244.7	0.0751	
			344.3	0.2660	
			411.1	0.0223	
			444.0	0.0312	
			778.9	0.1300	
			867.4	0.0421	
			964.1	0.1460	
			1085.9	0.0992	
			1112.1	0.1360	
			1408.0	0.2080	
^{203}Hg	46.58 d	684 ± 41	279.2	0.8150	01/05/1996
^{207}Bi	33.40 yr	426 ± 34	569.7	0.9780	01/11/1981
			1063.7	0.7490	
			1770.2	0.0685	
^{226}Ra	1600 yr	369 ± 15	2118.6	0.0121	01/09/1997
			2204.2	0.0499	
			2447.9	0.0155	

where a_0, a_1, a_2 and a_3 are fit parameters, while E_r is the energy reference value, which is constant. Fig. 5 shows the result of this fit.

Finally, the intrinsic efficiency of the HPGe detector was determined as function of the gamma-ray energy and, therefore, the values of this efficiency at the gamma-ray energies of interest were calculated, with the results presented in Table 5. The uncertainty associated with these efficiencies were calculated by covariance.

3.3. Measurement of the areas a_j

During gamma-ray spectroscopy measurements, the detection solid angle defines the fuel area from which gamma spectra are obtained [17]. In the measurements on irradiated MTR fuel elements, the detection solid angle defines a circle with area a_j on the central plane of the jth plate meat of a given irradiated fuel element. The measurement of the absolute gamma activity of an irradiated fuel element due to a burnup monitor requires the determination of each one of these areas. Analytical calculation of the a_j values is not feasible, since: (a) the collimator tube structure is rather complex (see Fig. 4); (b) a perfect alignment of collimating apertures of the upper and bottom collimators is very difficult to achieve (both collimating apertures have a diameter of 0.455 cm and in the collimator tube they are 288.10 cm apart).

Table 4
Obtained values for the intrinsic efficiencies ε_γ as function of the gamma-ray energies E_γ emitted by the calibration sources

E_γ (keV)	ε_γ
121.8	0.410 ± 0.013
122.0	0.388 ± 0.016
136.5	0.397 ± 0.016
160.6	0.349 ± 0.028
223.1	0.311 ± 0.026
244.7	0.324 ± 0.013
276.4	0.264 ± 0.013
279.2	0.287 ± 0.023
302.9	0.248 ± 0.012
344.3	0.228 ± 0.008
356.0	0.214 ± 0.011
383.9	0.210 ± 0.011
411.1	0.203 ± 0.014
444.0	0.177 ± 0.012
569.7	0.136 ± 0.011
661.6	0.1249 ± 0.0050
778.9	0.1114 ± 0.0048
834.8	0.1032 ± 0.0042
867.4	0.1001 ± 0.0072
898.0	0.0969 ± 0.0029
964.1	0.0952 ± 0.0039
1063.7	0.0797 ± 0.0064
1085.9	0.0896 ± 0.0047
1112.1	0.0766 ± 0.0037
1173.2	0.0762 ± 0.0031
1274.6	0.0750 ± 0.0030
1332.5	0.0674 ± 0.0027
1408.0	0.0690 ± 0.0028
1770.2	0.0518 ± 0.0044
1836.1	0.0527 ± 0.0016
2118.6	0.0522 ± 0.0070
2204.2	0.0584 ± 0.0040
2447.9	0.0501 ± 0.0062

It is necessary, therefore, to measure the a_j values directly.

The experimental arrangement for performing these measurements is shown in Fig. 6. In this setup, the collimator tube was positioned horizontally over holders. The HPGe detector, once installed inside the shielding, reproduces exactly the geometrical configuration of the detection set (collimator tube + HPGe detector) during the measurements on irradiated fuel elements at the reactor pool area.

In front of the opposite end of the collimator tube, the arrangement has a platform for moving

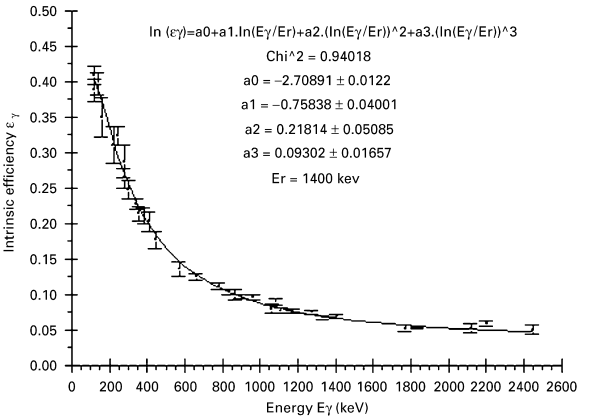

Fig. 5. Measured intrinsic efficiency for the HPGe detector, showing the function fitted to the experimental data.

Table 5
Intrinsic efficiency ε_γ of the HPGe detector at the main gamma-ray energies emitted by burnup monitors

Burnup monitor	E_γ (keV)	ε_γ
^{137}Cs	661.6	0.1249 ± 0.0050
^{95}Zr	724.2	0.1176 ± 0.0015
	756.7	0.1129 ± 0.0014
^{140}Ba/^{140}La	1596.5	0.0605 ± 0.0009
^{144}Ce/^{144}Pr	2185.7	0.0500 ± 0.0016

and precise positioning of a strong ^{137}Cs of known activity. When the source is exposed, a high collimated and intense gamma beam derives from a cylindrical opening (with diameter $\phi = 1.875$ cm) located in its front part. The measured source activity [9] was $A = (2.063 \pm 0.042) \times 10^{10}$ Bq.

The source is positioned and centralized in front of the bottom collimator. The areas a_j were measured in this configuration. The distances between the bottom collimator window and the front part of the source were adjusted to reproduce the relative positioning between the bottom collimator window and the center of each plate meat of a fuel element during the measurements performed at the reactor pool.

For each distance, a gamma spectrum was measured. A total of three complete sets of measurements were performed. In each one of these spectra, the net number of counts (Area) under the full-energy peak that corresponds to the gamma-ray of

Fig. 6. Photograph of the experimental arrangement used in order to measure the areas a_j.

661.6 keV was determined using the computer code IDEFIX [14].

Finally, the areas a_j were obtained by means of the following expression:

$$a_j = \frac{\text{Area} - j}{(A/\pi r^2)TI_\gamma \varepsilon_\gamma e^{-\mu_{Al}C_2} e^{-\mu_{air}(L+d_j)}} \quad (17)$$

where $\text{Area} - j$ is the average value of the area under the full-energy peak of 661.6 keV for the jth distance, $A = (2.063 \pm 0.042) \times 10^{10}$ Bq is the source activity, $r = \phi/2 = 0.9375$ cm is the radius of the opening outlet situated at the front part of the source, $T = 600$ s is the live time of each measurement, $I_\gamma = 0.851$ is the absolute emission intensity for the gamma-ray of 661.6 keV in the decay of ^{137}Cs, $\varepsilon_\gamma = (0.1249 \pm 0.0050)$ is the intrinsic efficiency of the HPGe detector at the energy of 661.6 keV, $\mu_{Al} = (0.2009 \pm 0.0007)\,\text{cm}^{-1}$ is the linear attenuation coefficient of aluminum for gamma-rays of 661.6 keV [18], $\mu_{air} = 9.4868 \times 10^{-5}\,\text{cm}^{-1}$ is the linear attenuation coefficient of air for gamma-rays of 661.6 keV [19], $C_2 = 0.100$ cm is the thickness of the aluminum window, $L = 327.40$ cm is the total length of the collimator tube and d_j is the jth distance adjusted between the aluminum window of the bottom collimator and the front part of the ^{137}Cs source, given by the equation

$$d_j = C_1 + [37 - 2j][a + (s/2)] + [18 - j]b, \quad (18)$$

Table 6
Measured values of a_j

j	d_j (cm)	a_j (10^{-9} cm^2)
1	8.073	(2.46 ± 0.22)
2	7.632	(2.52 ± 0.07)
3	7.191	(2.62 ± 0.08)
4	6.750	(2.56 ± 0.12)
5	6.309	(2.56 ± 0.09)
6	5.868	(2.75 ± 0.10)
7	5.427	(2.82 ± 0.12)
8	4.986	(2.80 ± 0.13)
9	4.545	(3.01 ± 0.19)
10	4.104	(2.90 ± 0.12)
11	3.663	(2.93 ± 0.26)
12	3.222	(3.02 ± 0.15)
13	2.781	(3.10 ± 0.23)
14	2.340	(2.92 ± 0.31)
15	1.899	(2.78 ± 0.12)
16	1.458	(2.96 ± 0.22)
17	1.017	(2.83 ± 0.21)
18	0.576	(3.07 ± 0.18)

where C_1 is the distance between the bottom collimator window and the last (18th) fuel plate of an element during the measurements at the reactor pool, a is the aluminum cladding thickness, s is the plate meat thickness, b is the distance between two successive fuel plates of an element and j is the index that designate the fuel plate (see part 2, Section 2.1, specially Figs. 1 and 2).

The values obtained for the areas a_j are shown in Table 6. It should be emphasized that, in this

experiment, the measured value of a_j is the effective projected area onto the central plane of the jth plate meat, which takes into account also eventual effects due to misalignment of collimating apertures inside the collimator tube.

3.4. Survey of the fuel elements characteristics

After the parameters ε_γ and a_j were measured, a survey was leaded to determine the main characteristics of the irradiated fuel elements selected for burnup measurements.

The operation registers of the IEA-R1 reactor were examined in order to reconstruct the irradiation history and the last irradiation date of each selected fuel element.

Besides, the mechanical project of each selected fuel element was consulted to obtain the parameters which are relevant to gamma-ray spectroscopy. A summary containing the results of these researches are shown in Table 7. Also important are the properties of structural materials of the fuel elements, water and air concerning the attenuation of gamma-rays. These properties are joined in Table 8 for the most important gamma-ray energies emitted in the decay of burnup monitors [13,18–20].

3.5. Gamma-ray spectroscopy measurements on irradiated fuel elements

The detection set (collimator tube + HPGe detector) was positioned over an aluminum base fixed at the pool border of the IEA-R1 research reactor, and equipped with two perpendicular crank driven mechanisms forming a x–y frame that enables the movement of the detection set either parallel or normal to the axial direction of an irradiated fuel element horizontally positioned.

In order to perform the gamma-ray spectroscopy measurements, an irradiated fuel element previously selected was hoisted up from the spent fuel storage rack (located at the bottom of the reactor pool) and brought to an immerse stainless steel platform, where it was positioned horizontally with the fuel plates surface-upwards. Reproducibility in the positioning of the irradiated fuel element was assured by an angle steel welded at the platform ground. Gamma-ray spectroscopy measurements

Table 7
Project parameters of the standard MTR fuel elements irradiated in the IEA-R1 research reactor

Fuel element identification	Manufacturer	Meat material	Initial enrichment (%)	Total number of plates	Active width (w) (cm)	Active length (l) (cm)	Meat thickness (s) (cm)	Cladding thickness (a) (cm)	Gap between plates (b) (cm)
Standard fuel elements									
80–112	UNC (USA)	U–Al alloy	93.15	18	6.350	59.7	0.0510	0.0505	0.289
IEA-123–IEA-127	NUKEM (Germany)	U–Al_x alloy in Al	19.75	18	6.035	59.0	0.0760	0.0380	0.289
IEA-130–further	IPEN (Brazil)	Dispersion U_3O_8 in Al	19.75	18	6.035	59.0	0.0760	0.0380	0.289

Table 8
Gamma-ray energies of interest (E_γ) and corresponding values of the mass attenuation coefficient (μ/ρ), density (ρ) and linear attenuation coefficient (μ) for aluminum, water, air and meat materials [13,18–20]

E_γ (keV)	Material	μ/ρ (cm^2/g)	ρ (g/cm^3)	μ (cm^{-1})
661.6	Al	0.07436 ± 0.00025	2.702	0.2009 ± 0.0007
	H_2O	0.0866	0.9982	0.0864
	Air	0.07776	0.00122	$9.4868.10^{-5}$
	U–Al alloy	0.0837 ± 0.0002	5.744	0.4808 ± 0.0011
	U–Al_x alloy in Al	0.0959 ± 0.0003	9.732	0.9330 ± 0.0025
	Dispersion U_3O_8 in Al	0.0982 ± 0.0004	4.1 ± 0.2	0.403 ± 0.020
724.2	Al	0.0734	2.702	0.1983
	H_2O	0.0835	0.9982	0.0834
	Air	0.07497	0.00122	$9.1463.10^{-5}$
	U–Al alloy	0.0802	5.744	0.4607
	U–Al_x alloy in Al	0.0891	9.732	0.8672
	Dispersion U_3O_8 in Al	0.0908 ± 0.0004	4.1 ± 0.2	0.372 ± 0.018
756.7	Al	0.0720	2.702	0.1946
	H_2O	0.0819	0.9982	0.0818
	Air	0.07354	0.00122	$8.9719.10^{-5}$
	U–Al alloy	0.0779	5.744	0.4475
	U–Al_x alloy in Al	0.0856	9.732	0.8328
	Dispersion U_3O_8 in Al	0.0870 ± 0.0003	4.1 ± 0.2	0.357 ± 0.017
1596.5	Al	0.04808 ± 0.00016	2.702	0.1299 ± 0.0004
	H_2O	0.0559	0.9982	0.0558
	Air	0.05034	0.00122	$6.1415.10^{-5}$
	U–Al alloy	0.0489 ± 0.0002	5.744	0.2809 ± 0.0011
	U–Al_x alloy in Al	0.0500 ± 0.0001	9.732	0.4862 ± 0.0014
	Dispersion U_3O_8 in Al	0.0503 ± 0.0002	4.1 ± 0.2	0.206 ± 0.010
2185.7	Al	0.0414	2.702	0.1119
	H_2O	0.0467	0.9982	0.0466
	Air	0.04214	0.00122	$5.1411.10^{-5}$
	U–Al alloy	0.0424	5.744	0.2435
	U–Al_x alloy in Al	0.0438	9.732	0.4258
	Dispersion U_3O_8 in Al	0.0440 ± 0.0002	4.1 ± 0.2	0.1804 ± 0.0088

were performed in the configuration shown schematically in Fig. 7.

In this configuration, the distance between the bottom collimator window and the last plate of the fuel element was determined using a scale and a radiation-resistant underwater camera. The distance measured was $C_1 = (0.60 \pm 0.05)$ cm. This value is compatible with the distance $d_{18} = 0.576$ cm (see part 3, Section 3.3) and with recommendations [21] that the reproducibility of the relative positioning between the bottom collimator window and the last plate of the fuel element must be assured within an error lower than ± 0.16 cm.

Fig. 8 presents a photograph of the gamma-ray spectroscopy system, where an irradiated fuel element positioned for measurement at the central point is shown.

In order to identify the full-energy peaks present in every gamma-ray spectrum obtained, an energy calibration of the HPGe detector was carried out immediately after the measurements.

Once the gamma-ray energy corresponding to the adequate burnup monitor was located, the net area under its full-energy peak was determined by means of the computer code IDEFIX [14]. Using this value of the area, the parameter $\overline{Q}$ was

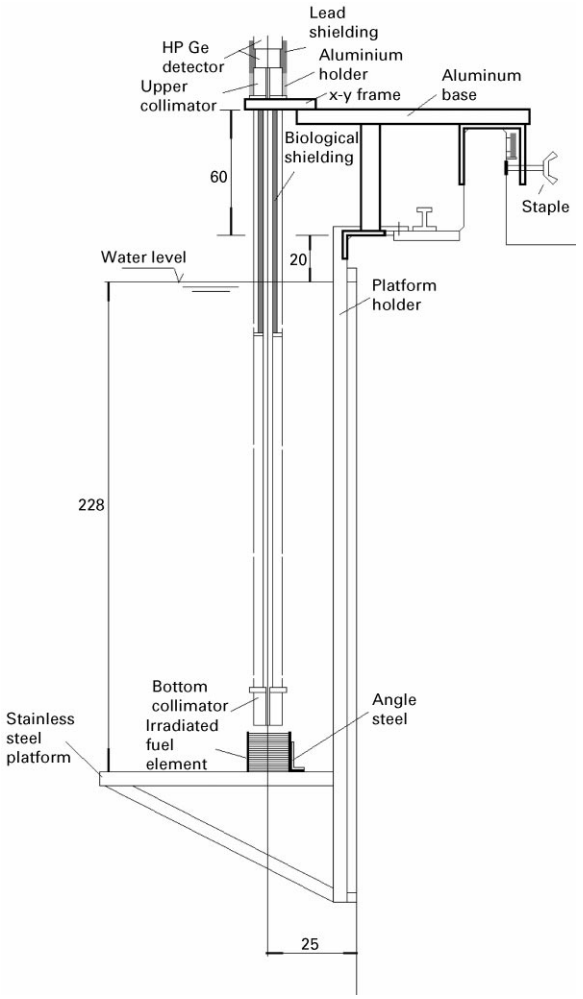

Fig. 7. Cross-sectional diagram of the experimental apparatus for gamma-ray spectroscopy installed at the pool area of the IEA-R1 research reactor. Dimensions are given in cm.

Fig. 8. Photograph of the detection set positioned for measurement at the central point of an irradiated fuel element.

calculated and thereafter the total activity of the irradiated fuel element due to the burnup monitor, as well as the fissioned mass of ^{235}U. Finally, the ratio of the fissioned to the original mass of ^{235}U of an irradiated fuel element furnished its burnup.

4. Results and discussion

After the pool background measurements were performed, full-energy peaks in the corresponding gamma spectrum were identified using the energy calibration. No fission products at all were found. Only activation products and some isotopes of the natural background [22] were detected [9].

Among the activation products, ^{58}Co ($T_{1/2} = 70.92$ d), ^{60}Co ($T_{1/2} = 5.27$ yr) and ^{65}Zn ($T_{1/2} = 244.1$ d) are always present in water samples collected from the reactor pool [6]. They are generated by oxidation (chemical reaction) and neutron absorption (nuclear reaction) occurred at the cladding and holders of the reactor control rods, both made of metallic nickel (cases of ^{58}Co and ^{60}Co), or at structures of the heat exchangers (case of ^{65}Zn).

However, if the pool water sample is collected with the reactor under operation or thereupon the reactor shutdown, the activation product ^{24}Na ($T_{1/2} = 15.02$ h) is largely predominant. It is

Table 9
Magnitude of the corrections due to attenuation effects for each gamma-ray spectroscopy measurement on standard fuel elements. The magnitude of F_j was evaluated considering all plates of the fuel element (see part 2, Section 2.1)

Fuel element	Burnup monitor	E_γ (keV)	k_1 (%)	k_2 (%)	k_3 (%)	F_j (%)
84, 88, 91, 92, 93, 96, 98, 101, 105, 107, 108, 111, 112	^{137}Cs	661.6	1.2	8.6	3.2	66.7
86	^{144}Ce/^{144}Pr	2185.7	0.6	4.6	1.7	33.3
IEA-123, IEA-124, IEA-126	^{137}Cs	661.6	3.6	8.3	3.2	113.4
IEA-130, IEA-131, IEA-132	^{144}Ce/^{144}Pr	2185.7	0.7	4.4	1.7	31.9

generated by the nuclear reaction ^{27}Al(n,α)^{24}Na, occurred in the aluminum cladding of fuel and reflector elements, as well as in aluminum structures of the reactor core, during the irradiation [6].

Finally, the activation product ^{110m}Ag ($T_{1/2} = 249.9$ d) is generated by means of radiative capture of one neutron by the isotope ^{109}Ag, which forms 48.17% of the natural silver [4], metal that constitutes 80% of the alloy used in the reactor control rods. This silver, activated in the reactor core, dilutes in the pool water as monovalent cations, once the silver oxide is slightly soluble [23]. However, on the contrary of the other activation products, ^{110m}Ag is not detected in pool water samples, but in metallic surfaces over which this isotope is deposited probably by means of displacement chemical reactions. Hence, ^{110m}Ag was detected over the aluminum cladding surface of the fuel plates of almost all stored fuel elements [6].

The pool background measurement also demonstrated that prominent Compton continua from high-energy gamma-rays, mainly the ones emitted in the decay of activation products, can obscure full-energy peaks from gamma-rays emitted in the decay of burnup monitors and, as a consequence, would distort the result of the gamma-ray spectroscopy measurements on irradiated fuel elements. Once the most important activation product concerning this issue is ^{24}Na, it was decided that gamma-ray spectroscopy measurements on irradiated fuel elements would be performed only during long maintenance periods in which the reactor did not operate.

Initially, the irradiated fuel elements, selected for gamma-ray spectroscopy measurements, were assorted in two groups, according to the cooling time and fission product used as burnup monitor. Fuel elements with cooling times equal or longer than two years were monitored using ^{137}Cs, whereas for shorter cooling times the utilized burnup monitor was ^{144}Ce/^{144}Pr. The fission products ^{95}Zr and ^{140}Ba/^{140}La could not be used as burnup monitors because all selected fuel elements were irradiated in the reactor core for a period much longer than 200 d.

Thereafter, corrections due to attenuation effects (see part 2, Section 2.1) were previously calculated in order to evaluate their magnitude for each measurement to be performed on standard fuel elements, with the results shown in Table 9.

Correction factors regarding the irradiation history of the standard fuel elements selected for measurement (see part 2, Section 2.2 and part 3, Section 3.4) were also calculated, with the results shown in Table 10.

Considering their importance, both corrections were used in all measurements.

The duration of a gamma-ray spectroscopy measurement at each selected point varied according to the burnup monitor employed. If the chosen burnup monitor was ^{137}Cs, each measurement had the duration of 600 s of live time. However, if the suitable burnup monitor was ^{144}Ce/^{144}Pr, each measurement had the duration of 3600 s of live time. A gamma-ray spectrum was obtained from each measurement. As a consequence, complete gamma-ray spectra were accumulated as a function of axial and transversal positions for a given irradiated fuel element.

An additional test of the experimental method was performed later, measuring the burnup of two partial fuel elements manufactured by IPEN and irradiated in the IEA-R1 reactor. These partial fuel elements present the same project parameters of the

Table 10
Correction factor regarding the irradiation history of each standard fuel element selected for gamma-ray spectroscopy measurement (see part 2, Section 2.2, specially Eq. (13) and part 3, Section 3.4)

Fuel element	Burnup monitor	f
84	^{137}Cs	1.46
86	^{144}Ce/^{144}Pr	10.81
88	^{137}Cs	1.23
91	^{137}Cs	1.34
92	^{137}Cs	1.14
93	^{137}Cs	1.31
96	^{137}Cs	1.28
98	^{137}Cs	1.30
101	^{137}Cs	1.17
105	^{137}Cs	1.22
107	^{137}Cs	1.21
108	^{137}Cs	1.19
111	^{137}Cs	1.21
112	^{137}Cs	1.18
IEA-123	^{137}Cs	1.17
IEA-124	^{137}Cs	1.17
IEA-126	^{137}Cs	1.18
IEA-130	^{144}Ce/^{144}Pr	6.07
IEA-131	^{144}Ce/^{144}Pr	5.82
IEA-132	^{144}Ce/^{144}Pr	4.50

standard ones also fabricated by IPEN (see part 3, Section 3.4, specially Tables 7 and 8), except for the total number of fuel plates: the fuel element IEA-128 has two fuel plates (the first and the 18th ones), whereas the fuel element IEA-129 has 10 fuel plates (the first, 3rd, 5th, 7th, 9th, 10th, 12th, 14th, 16th and 18th ones). The other fuel plates of these elements were replaced by massive aluminum plates of the same thickness. Each measurement on these partial fuel elements was longer than corresponding ones performed on standard fuel elements also monitored using ^{137}Cs, requiring 900 s of live time (IEA-129) and 1200 s of live time (IEA-128).

As an example of gamma spectra obtained from measurements on irradiated fuel elements monitored with ^{137}Cs, Fig. 9 shows the gamma spectrum from a run of 600 s of live time carried out at the central point of the fuel element 111.

It is important to observe that the full-energy peak from 661.6 keV, that corresponds to the gamma-ray emitted in the decay of ^{137}Cs, is the most prominent in the gamma spectrum.

For each gamma spectrum obtained from measurements performed along the active width

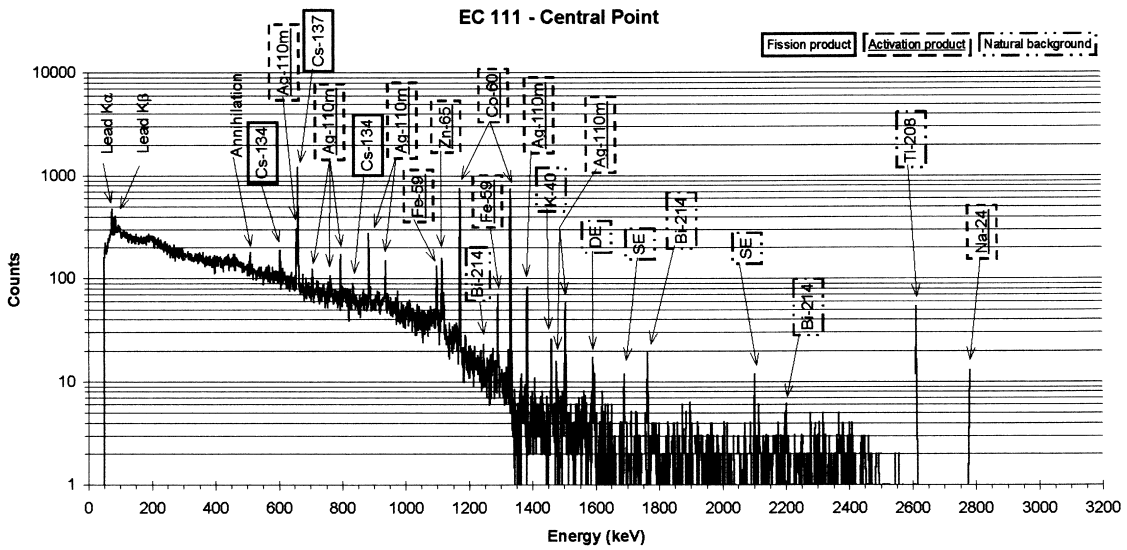

Fig. 9. Gamma-ray spectrum obtained from measurement of 600 s of live time performed at the central point of the irradiated fuel element 111. The origin of each peak is indicated.

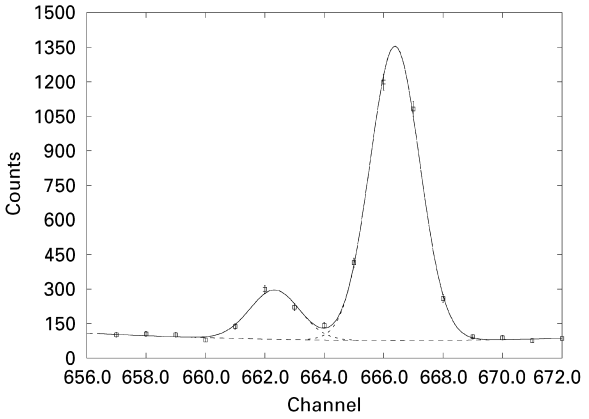

Fig. 10. Gaussian functions fitted to each full-energy peak of the doublet with energies 657.7 keV (^{110m}Ag) and 661.6 keV (^{137}Cs) using the computer code IDEFIX [14], in order to separate the areas of these peaks in the gamma-ray spectrum obtained from measurement at the central point of the fuel element 111.

and along the active length of an irradiated fuel element, the net number of counts (area) under the full-energy peak from 661.6 keV was determined using the computer code IDEFIX [14].

In every gamma spectra, the full-energy peak from 661.6 keV is always preceded by another one, much smaller and very close, identified as correspondent to the most intense gamma-ray emitted in the decay of the activation product ^{110m}Ag ($E_\gamma = 657.7$ keV, $I_\gamma = 0.947$). Hence, it was necessary to fit a Gaussian function to each one of the full-energy peaks of a doublet using the computer code IDEFIX [14], in order to separate correctly their areas, as shown in Fig. 10.

The areas under the full-energy peaks from 661.6 keV, presented as a function of the active length and active width of an irradiated fuel element, constitute its burnup profiles. As an example, Fig. 11 shows the burnup profiles for the fuel element 111.

The values of the areas were used in order to calculate the parameter $\overline{Q}$ and, thereafter, the total activity of an irradiated fuel element due to the burnup monitor ^{137}Cs, as well as the fissioned mass of ^{235}U in this fuel element (see part 2, Section 2.2). Finally, the ratio between fissioned and initial masses of ^{235}U in this fuel element furnishes its

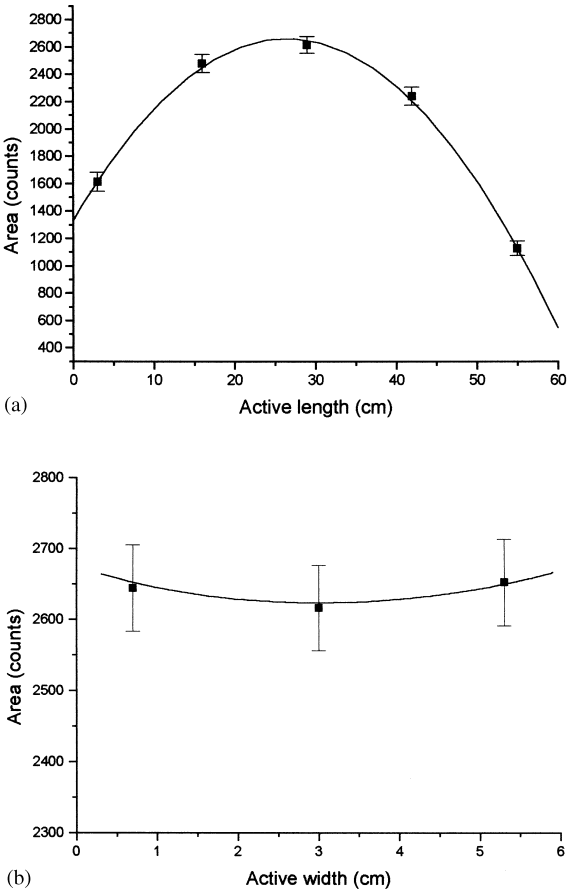

Fig. 11. Experimental burnup profiles for the fuel element 111: (a) burnup profile along the active length; (b) burnup profile along the active width. The curves joining the points are just to guide the eye.

burnup. All these calculations employed to determine burnup from experimental data were made using the software EXCEL [24].

A resembling procedure was adopted for measurements on irradiated fuel elements monitored with ^{144}Ce/^{144}Pr, but in this case each selected point was measured during 3600 s of live time. Fig. 12 shows the gamma spectrum from a measurement carried out at the central point of the fuel element IEA-131.

In this spectrum, one observes many full-energy peaks from gamma-rays emitted in the decay of short-lived fission products, like ^{95}Zr, ^{95}Nb, ^{103}Ru, ^{106}Rh and also the adopted burnup monitor ^{144}Pr,

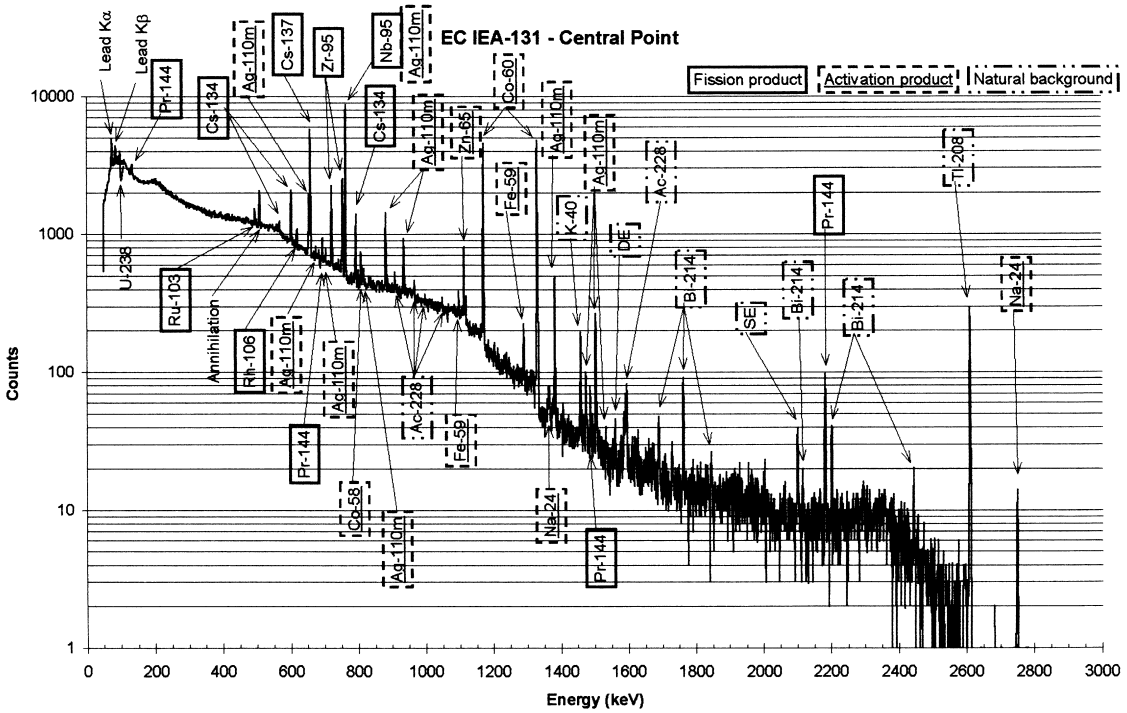

Fig. 12. Gamma-ray spectrum obtained from measurement of 3600 s of live time performed at the central point of the irradiated fuel element IEA-131. The origin of each peak is indicated.

whose full-energy peak from 2185.7 keV arises isolated and very clearly. The burnup profiles for the fuel element IEA-131 are shown in Fig. 13.

Once finished the measurements on every irradiated fuel elements previously selected, the obtained burnup values were directly compared with corresponding ones provided by reactor physics calculations [8,25], with the results shown in Table 11.

Concerning standard fuel elements, the average relative experimental uncertainty for measurements monitored with ^{137}Cs is 7.5%, whereas for measurements monitored with ^{144}Ce/^{144}Pr this uncertainty reaches 16.3%.

The lower precision obtained in burnup measurements monitored with ^{144}Ce/^{144}Pr is a consequence of the low absolute emission intensity for the high-energy gamma-ray analyzed ($E_\gamma = 2185.7$ keV, $I_\gamma = 0.007$), which enhances the uncertainty of the area under the corresponding full-energy peak, because the total number of detected gamma-rays and therefore of recorded counts tend to be low at this energy. Relative experimental uncertainties up to 30% were obtained measuring with ^{144}Ce/^{144}Pr the burnup of nuclear fuels irradiated at power reactors [26,27].

Using the data exposed in Table 11, the ratio gamma-ray spectroscopy/reactor physics calculations was determined for each fuel element burnup, with the results shown in Fig. 14. For most fuel elements, a good agreement within the experimental error limits is observed.

Other burnup measurements performed recently exhibit analogous results.

Measurements carried out using a planar minidetector of cadmium telluride (CdTe) and employing the ratio of ^{134}Cs and ^{137}Cs activities together with isotopic correlations, furnished burnup results that, compared with the ones declared by the reactor operators, agree within an uncertainty of 10% [28].

On the other hand, a compilation embracing a very large number of burnup measurements

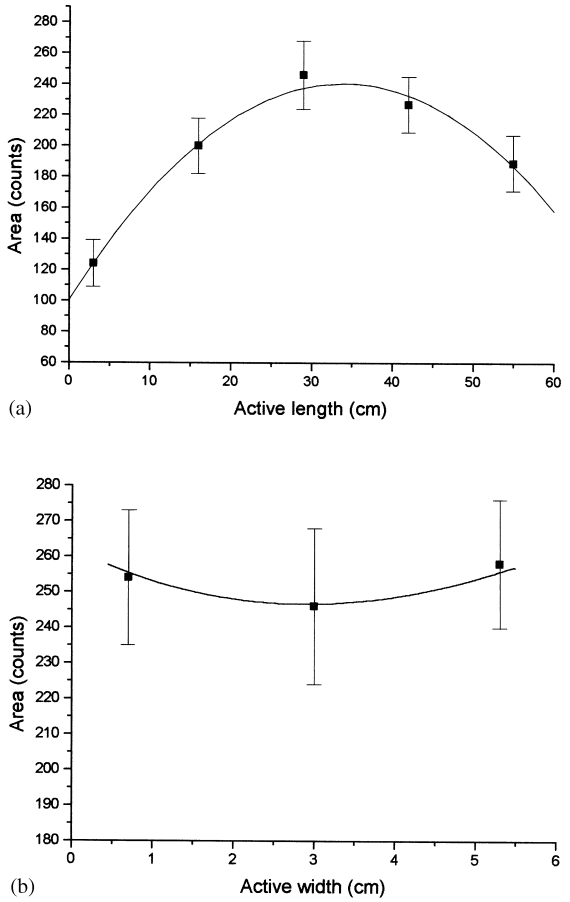

Fig. 13. Experimental burnup profiles for the fuel element IEA-131: (a) burnup profile along the active length; (b) burnup profile along the active width. The curves joining the points are just to guide the eye.

monitored with ^{137}Cs, and performed on nuclear fuels irradiated at power reactors, shows results that, compared with corresponding ones provided by reactor physics calculations, differ at the utmost by 8% [29].

5. Conclusion

Absolute burnup of several MTR fuel elements, irradiated in the IEA-R1 research reactor, was determined by nondestructive gamma-ray spectroscopy measurements.

The performed measurements embrace three kinds of standard fuel elements with different cooling times and initial enrichment grades, as well as two partial fuel elements.

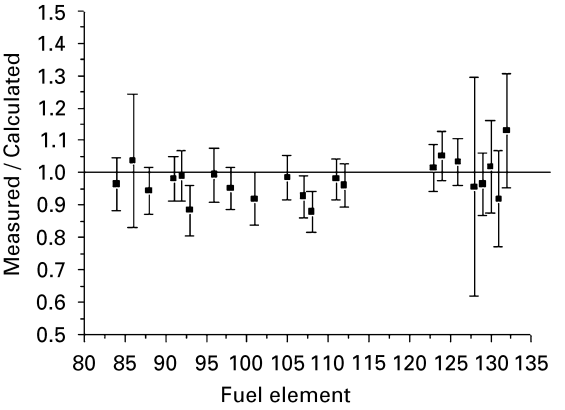

Fig. 14. Ratio of measured/calculated burnup values for each fuel element.

Fuel elements with cooling times equal or longer than two years were monitored using ^{137}Cs, whereas for shorter cooling times the utilized burnup monitor was ^{144}Ce/^{144}Pr.

The obtained burnup values were compared with corresponding ones provided by reactor physics calculations and good agreement within the experimental error limits was observed between them.

The technique and experimental apparatus employed in this work are rather simple and provide by nondestructive analysis a considerable amount of reliable information, never obtained before, about the fuel elements irradiated in Brazilian research reactors.

Acknowledgements

The authors would like to express their gratitude to Roberto Frajndlich, chief of the IEA-R1 Operation Division, whose participation was indispensable to achieve the objectives of this research. Special acknowledgment is owed to the IEA-R1 operators for the handling of irradiated fuel elements inside the reactor pool. One of the authors (C.A. Zeituni) gratefully acknowledges support from the Conselho Nacional de Desenvolvimento Científico e Tecnológico (CNPq).

Table 11
Burnup values obtained by means of gamma-ray spectroscopy measurements compared with corresponding ones provided by reactor physics calculations

Fuel element	Storage date (d/month/yr)	Burnup monitor	Gamma-ray spectroscopy (%)	Reactor physics calculations (%)
84	10/06/1996	^{137}Cs	45.2 ± 3.8	46.9
86	05/05/1997	^{144}Ce/^{144}Pr	50.2 ± 9.9	48.4
88	31/12/1986	^{137}Cs	38.3 ± 2.9	40.5
91	12/12/1994	^{137}Cs	46.8 ± 3.3	47.6
92	09/11/1981	^{137}Cs	37.2 ± 2.9	37.6
93	09/07/1992	^{137}Cs	35.3 ± 3.1	39.9
96	09/07/1992	^{137}Cs	40.3 ± 3.4	40.5
98	19/12/1994	^{137}Cs	46.0 ± 3.1	48.3
101	30/06/1989	^{137}Cs	35.9 ± 3.2	39.1
105	16/10/1995	^{137}Cs	46.7 ± 3.2	47.4
107	17/09/1994	^{137}Cs	44.8 ± 3.2	48.3
108	27/09/1993	^{137}Cs	40.6 ± 2.9	46.2
111	04/09/1995	^{137}Cs	46.4 ± 3.0	47.4
112	04/09/1995	^{137}Cs	44.5 ± 3.0	46.3
IEA-123	16/10/1995	^{137}Cs	46.6 ± 3.4	45.9
IEA-124	16/10/1995	^{137}Cs	48.0 ± 3.5	45.6
IEA-126	10/06/1996	^{137}Cs	47.7 ± 3.3	46.2
IEA-128[a]	07/01/1991	^{137}Cs	12.0 ± 4.3	12.6
IEA-129[a]	30/09/1993	^{137}Cs	17.8 ± 1.8	18.4
IEA-130	09/09/1997	^{144}Ce/^{144}Pr	36.8 ± 5.1	36.1
IEA-131	09/09/1997	^{144}Ce/^{144}Pr	28.9 ± 4.7	31.5
IEA-132	09/07/1997	^{144}Ce/^{144}Pr	30.9 ± 4.8	27.3

[a] Partial fuel elements.

References

[1] W.R. Diggle, W.H. Blackadder, Nucleonics 23 (3) (1965) 71.
[2] Reactor Burn-up Physics, IAEA Panel Proceedings Series, Vienna, 1973.
[3] U. Reus, W. Westmeier, At. Data Nucl. Data Tables 29 (1983) 1.
[4] U. Reus, W. Westmeier, At. Data Nucl. Data Tables 29 (1983) 193.
[5] JNDC Nuclear Data Library of Fission Products – Japan Atomic Energy Research Institute – JAERI 1287, Tokyo, 1983.
[6] J.A. Perrotta, L.A.A. Terremoto, C.A. Zeituni, Ann. Nucl. Energy 25 (1998) 237.
[7] A.G. Croff, Nucl. Technol. 62 (1983) 335.
[8] M. Yamaguchi, Validação da Metodologia de Cálculo Neutrônico do Reator IEA-R1, Technical Report, IPEN/CNEN-SP, São Paulo, 1997.
[9] C.A. Zeituni, Espectrometria Gama em Elementos Combustíveis Tipo Placa Irradiados, M.Sc. Dissertation, IPEN/CNEN-SP, São Paulo, 1998.
[10] A.J. Kestelman, S.R. Guevara, Determinacion del Quemado en Combustibles Tipo MTR Mediante Espectrometria Gama com Cristal INa(Tl), Technical Report, CNEA-CAB, Bariloche, 1988.
[11] Nuclear Safeguards Technology 1978 – Vol. I, IAEA-SM-231/135, Vienna, 1979.
[12] Quality Assurance Data Sheet – GEM Series HPGe (High-Purity Germanium) Coaxial Detector System, EG & G ORTEC, Oak Ridge, 1993.
[13] G.F. Knoll, Radiation Detection and Measurement, John Wiley & Sons, Inc., New York, 1989.
[14] P. Gouffon, IDEFIX – Manual do Usuário, Laboratório do Acelerador Linear/Instituto de Física da Universidade de São Paulo (LAL/IFUSP), São Paulo, 1983.
[15] O.Y. Mafra, Técnicas e Medidas Nucleares, Editora Edgard Blücher Ltda., São Paulo, 1973.
[16] K. Debertin, R.G. Helmer, Gamma- and X-Ray Spectrometry with Semiconductor Detectors, Elsevier Science Publishers B.V., Amsterdam, 1988.
[17] J.R. Phillips, G.R. Waterbury, G.H. Mottaz, J.N. Quintana, New System for Gamma Scanning Fuel Elements, Proceedings of 20th Conference on Remote Systems Technology, 1972, p. 115.
[18] A.L. Conner, H.F. Atwater, E.H. Plassman, J.H. McCrary, Phys. Rev. A1 (1970) 539.

[19] J.R. Lamarsh, Introduction to Nuclear Engineering, Addison-Wesley Publishing Company Inc., Reading, MA, 1977.
[20] CRC Handbook of Chemistry and Physics, 75th Edition, CRC Press Inc., Boca Raton, FL, 1994.
[21] Nuclear Materials Management, IAEA-SM-67/45, Vienna, 1966.
[22] R. Ejnisman, P.R. Pascholati, Rev. Física Aplicada Instrumentação 9 (1994) 139.
[23] N. Glinka, Química Geral – Vol. 2, Mir Publishers, Moscow, 1984.
[24] Microsoft EXCEL, Version 5.0c or higher, Microsoft Corporation, 1985–1994.
[25] Determination of Research Reactor Fuel Burnup, IAEA-TECDOC-633, Vienna, 1992.
[26] S.T. Hsue, At. Energy Rev. 16 (1) (1978) 89.
[27] J.D. Chen, D.G. Boase, R.B. Lypka, Non-Destructive Determination of Burn-Up by Gamma-Scanning: an Assessment of ^{144}Ce/Pr as a Fission Monitor in CANDU Fuels, Rep. AECL-5236, Atomic Energy of Canada Limited/Chalk River Nuclear Laboratories, Chalk River, 1976.
[28] K. Abbas, G. Nicolaou, D. Pellottiero, P. Schwalbach, L. Koch, Nucl. Instr. and Meth. A 376 (1996) 248.
[29] I. Matsson, B. Grapengiesser, Appl. Radiat. Isot. 48 (1997) 1289.